

# On the use of satellite-based estimates of rainfall temporal distribution to simulate the potential for malaria transmission in rural Africa

Teresa K. Yamana<sup>1</sup> and Elfatih A. B. Eltahir<sup>1</sup>

Received 9 July 2010; revised 22 November 2010; accepted 21 December 2010; published 23 February 2011.

[1] This paper describes the use of satellite-based estimates of rainfall to force the Hydrology, Entomology and Malaria Transmission Simulator (HYDREMATS), a hydrology-based mechanistic model of malaria transmission. We first examined the temporal resolution of rainfall input required by HYDREMATS. Simulations conducted over Banizoumbou village in Niger showed that for reasonably accurate simulation of mosquito populations, the model requires rainfall data with at least 1 h resolution. We then investigated whether HYDREMATS could be effectively forced by satellite-based estimates of rainfall instead of ground-based observations. The Climate Prediction Center morphing technique (CMORPH) precipitation estimates distributed by the National Oceanic and Atmospheric Administration are available at a 30 min temporal resolution and 8 km spatial resolution. We compared mosquito populations simulated by HYDREMATS when the model is forced by adjusted CMORPH estimates and by ground observations. The results demonstrate that adjusted rainfall estimates from satellites can be used with a mechanistic model to accurately simulate the dynamics of mosquito populations.

**Citation:** Yamana, T. K., and E. A. B. Eltahir (2011), On the use of satellite-based estimates of rainfall temporal distribution to simulate the potential for malaria transmission in rural Africa, *Water Resour. Res.*, 47, W02540, doi:10.1029/2010WR009744.

## 1. Introduction

[2] Malaria is responsible for nearly a million deaths each year, 90% of which occur in Africa [Aregawi *et al.*, 2008]. The disease is caused by the plasmodium parasite, which is transmitted primarily by *Anopheles* mosquitoes. In arid areas such as the Sahel, malaria is closely linked to rainfall, as the mosquitoes that transmit the disease are limited by the availability of vector breeding habitat. In Niger, the primary malaria vector is *Anopheles gambiae*, which breeds in temporary rainwater-fed pools on the order of tens of meters in diameter. The formation of these pools and their utilization by mosquitoes is mechanistically modeled by the Hydrology, Entomology and Malaria Transmission Simulator (HYDREMATS), developed by Bomblies *et al.* [2008]. HYDREMATS has been used in a number of studies of *Anopheles* mosquito dynamics in Bani-zoumbou and Zindarou villages in Niger [Bomblies *et al.*, 2008; Gianotti *et al.*, 2008a, 2008b; Bomblies and Eltahir, 2010].

[3] Previous applications of HYDREMATS relied on ground observations for rainfall forcings. This limits the use of the model, as rain gauge networks are sparse in many malaria-prone areas. The incorporation of satellite-based rainfall data into HYDREMATS would greatly increase the range of applicability of the model. As rainfall estimates from

satellites vary in their temporal resolution, it is important to determine the resolution required by HYDREMATS. Previous studies relating rainfall to malaria transmission have used temporal resolutions on the order of days for mechanistic models [Patz *et al.*, 1998; Hoshen and Morse, 2004] or months for statistical models [Craig *et al.*, 1999; Kilian *et al.*, 1999; Thomson *et al.*, 2005]. However, hydrology models require a much finer time scale. The main hydrological process of interest for malaria transmission is surface runoff, as this is an important process affecting the mechanism by which water forms pools of water that can be used by anopheles mosquitoes. Investigations of the temporal resolution requirements of runoff models have found that rainfall inputs on the order of minutes or hours are required [Finnerty *et al.*, 1997; Krajewski *et al.*, 1991; Pessoa *et al.*, 1993; Winchell *et al.*, 1998].

[4] The application of remote sensing approaches to malaria control has been the subject of extensive research over the past 30 years, as has been reviewed in numerous articles [Kalluri *et al.*, 2007; Ceccato *et al.*, 2005; Rogers *et al.*, 2002; Hay *et al.*, 1998a; Thomson *et al.*, 1996]. A common approach is to apply statistical techniques relating satellite images of land cover such as 30 m resolution data from Landsat satellites to mosquito abundance in order to create maps of suitable mosquito habitat [Beck *et al.*, 1994; Pope *et al.*, 1994; Diuk-Wasser *et al.*, 2004; Masuoka *et al.*, 2003]. Bogh *et al.* [2007] extended this approach to estimate the entomological inoculation rate (EIR), defined as the number of infectious bites per person, per unit time. Normalized difference vegetation index (NDVI) data from multispectral sensors such as the National Ocean and Atmospheric

<sup>1</sup>Ralph M. Parsons Laboratory, Massachusetts Institute of Technology, Cambridge, Massachusetts, USA.

Administration's (NOAA) advanced very high resolution radiometer (AVHRR), available at 1.1 km resolution, have been widely used as a proxy for rainfall data to map mosquito habitat suitability or malaria distribution [Hay et al., 1998b; Nihei et al., 2002; Eisele et al., 2003; Thomson et al., 1999; Rahman et al., 2006]. The NDVI value gives information on the abundance of green vegetation, which can then be used to infer information about rainfall [Thomson et al., 1996]. NDVI ranges from  $-1$  to  $1$  and is given by the formula  $NDVI = (NIR - RED)/(NIR + RED)$ , where NIR is percentage reflectance in the near-infrared channel and RED is the percentage reflectance in the red channel.

[5] Some authors have investigated satellite-based measurements of environmental variables directly. Thomson et al. [2005] found correlations between malaria incidence in Botswana and estimates of seasonal rainfall and sea surface temperature. Omumbo et al. [2002] examined the relationships between historical intensity of malaria transmission and NDVI, midinfrared reflectance, land surface temperature, and air temperature data obtained from AVHRR as well as data on altitude and cold cloud duration in Tanzania, Kenya, and Uganda.

[6] Monitoring rainfall has been recognized as an essential component for the malaria early warning systems advocated for by the Roll Back Malaria initiative [Grover-Kopec et al., 2005]. In response to this need, decadal (every 10 days) estimates of rainfall anomalies are distributed by the Africa Data Dissemination Service, a Web site supported by the U.S. Agency for International Development. The estimates incorporate rain gauge data with cloud top temperature from Meteosat 7 as well as estimates from the special sensor microwave/imager on the Defense Meteorological Satellite Program satellites and the advanced microwave sounding unit on NOAA satellites [Ceccato et al., 2006]. Hay et al. [2003] retrospectively determined that these data would have provided a reliable warning to a major malaria epidemic that occurred in 2002 in Kenya.

[7] While all of these studies use remote sensing data of some form, none use satellite-based estimates of meteorological variables to force a mechanistic model of malaria transmission such as HYDREMATS. Rogers et al. [2002] and Kalluri et al. [2007] call for the use of satellite data in mechanistic models of vector-borne pathogen transmission as an improvement over the statistical models currently being used and an important next step for malaria control. We propose the use of rainfall estimates from the Climate Prediction Center morphing method (CMORPH) in order to directly simulate the relationship between rainfall and mosquito populations. CMORPH was chosen because of its high spatial and temporal resolution and because CMORPH has been shown to perform significantly better at estimating rainfall than techniques that use only passive microwave (PMW) images or PMW data blended with rainfall estimates derived from infrared (IR) data [Joyce et al., 2004].

[8] CMORPH [Joyce et al., 2004] provides global estimates of rainfall every 30 min at a  $0.07277^\circ$  ( $\sim 8$  km) spatial resolution. CMORPH combines rainfall estimates from PMW sensors with spatial propagation vectors derived from IR data. PMW sensors can detect thermal emission and scattering patterns associated with rainfall. However, these sensors are only available on polar orbiting satellites, giving them limited spatial and temporal coverage. Infrared data

from geostationary satellites are available globally at 30 min resolution and can be used to determine the movements of the precipitating systems sensed by PMW instruments. CMORPH uses infrared measurements from the Geostationary Operational Environmental Satellites 8 and 10, Meteosat-5 and Meteosat-7, and Geostationary Meteorological Satellite-5. PMW sensors used by CMORPH are aboard the NOAA polar-orbiting operational meteorological satellites, the U.S. Defense Meteorological Satellite Program satellites, and the Tropical Rainfall Measuring Mission (TRMM) satellite. Consecutive PMW images are propagated forward and backward in time using motion vectors derived from the infrared images. The shape and intensity of the precipitating systems in the 30 min intervals between PMW measurements are determined by using a time-weighted linear interpolation [Joyce et al., 2004]. CMORPH has been found to significantly overestimate rainfall in Africa [Laws et al., 2004]. The wet bias of CMORPH data has been attributed to evaporation of rainfall below the cloud base [Tian and Peters-Lidard, 2007].

## 2. Study Area

[9] The simulations in this paper were conducted over the domain of our field site, Banizoumbou village in southwestern Niger. Banizoumbou is a typical Sahelian village in a semiarid landscape, with a population of about 1000. Land cover consists of tiger bush shrubland, millet fields, and fallow and bare soil. Millet fields dominate near the village, while tiger bush is more common near surrounding plateau tops [Bomblies et al., 2008]. The rainy season in Banizoumbou extends from May to October, with maximum rainfall occurring in August. During this time, water pools form in and around the village, providing ideal breeding habitat for *A. gambiae* mosquitoes. Mosquito populations and malaria transmission in Niger increase dramatically during the rainy season.

[10] Meteorological data from three additional West African locations were used to calibrate CMORPH data: Zindarou village in Niger, Djougou in Benin, and Agoufou in Mali. Zindarou village is located approximately 20 km away from Banizoumbou. Djougou, Benin, receives significantly more rainfall than Banizoumbou, with an average of over 1000 mm/yr, spread out over a longer rainy season. Agoufou, Mali, is notably drier than Banizoumbou, with average annual rainfall between 200 and 400 mm. The map depicted in Figure 1 shows the four locations. The dotted contour lines show average annual rainfall.

## 3. HYDREMATS Model Description

[11] The development of the Hydrology, Entomology and Malaria Transmission Simulator (HYDREMATS) is described in detail by Bomblies et al. [2008]. The model was developed to simulate village-scale response of malaria transmission to climate variability in semiarid desert fringe environments such as the Sahel. The model provides explicit representation of the hydrology and mosquito life cycle, which are important determinants of malaria transmission. HYDREMATS can be separated into two components: the hydrology component, which explicitly represents water pools available to anopheles mosquitoes as breeding sites, and the entomology component, which is an agent-based model of the *Anopheles* mosquito life cycle.

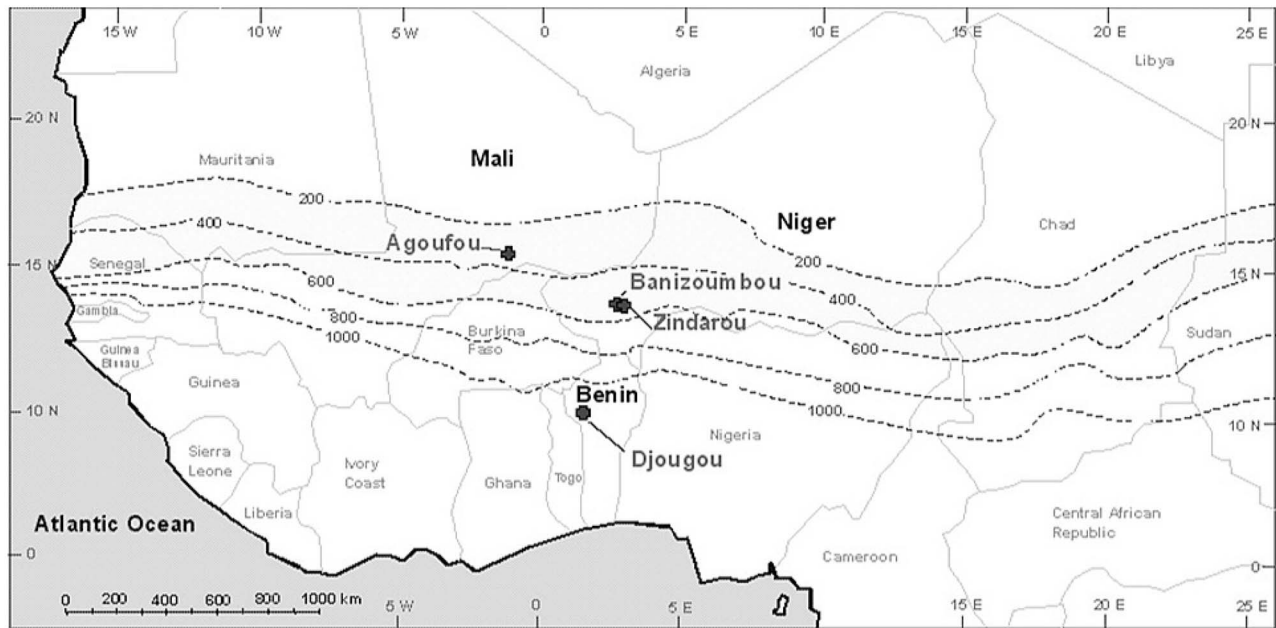


**Figure 1.** Locations of Banizoumbou, Zindarou, Agoufou, and Djougou (adapted from *Bomblies et al.* [2008]).

[12] The hydrology component of HYDREMATS is based on the land surface scheme LSX of *Pollard and Thompson* [1995]. The model simulates momentum, energy, and water fluxes within its vertical column of the atmosphere, six soil layers, and two vegetation layers. Vegetation type and soil characteristics are required as model inputs and strongly influence soil moisture and runoff in the model. Thicknesses and permeabilities of vertical soil layers are assigned to represent the soil structure observed in the Sahel, including the thin layer of low-permeability crust commonly observed in areas with sparse vegetation [*Bomblies et al.*, 2008].

[13] Water at each grid cell is partitioned between runoff and infiltration on the basis of a Hortonian runoff process governed by hydraulic conductivity and porosity of the soil. Unsaturated zone hydraulic conductivity is calculated as a function of soil moisture following Campbell's equation. Infiltration through the unsaturated zone is calculated using an implicit Richard's equation solver. Uptake of soil water from evapotranspiration is calculated on the basis of climatic variables. Overland flow is modeled using a finite difference solution of a diffusion wave approximation to the St. Venant equations following the formulation of *Lal* [1998]. Flow velocity is represented by Manning's equation as a function of friction slope, flow depth, and the distributed roughness parameter  $n$ , which is derived from soil characteristics and vegetation type. The overland flow process is of critical importance for the modeling of water pool formation [*Bomblies et al.*, 2008].

[14] The meteorological inputs required by the model are temperature, humidity, wind speed and direction, incoming solar radiation, and rainfall. These variables are assumed to be uniform over the model domain in the simulations conducted in this paper. Distributed rasters of vegetation, soil type, and topography are required at the grid resolution specified by the user. The hydrology component of HYDREMATS generates a grid of water depths and temperatures for each grid cell for each time step. These grids

serve as the inputs for the entomology component of the model [*Bomblies et al.*, 2008]. HYDREMATS output rasters of pool water depths for each time step can be compared to assess the effect of reducing temporal resolution on the modeling of pool formations. Figure 2 shows a sample raster of pool depths for the 2.5 km by 2.5 km model domain. Each grid point has dimensions of 10 m by 10 m. The three labeled pools correspond to three grid points for which a time series of pool depths is simulated by the model and examined. Pool 1 is a large pool on the outskirts of the village. Mosquito larvae are not generally found in pools of this size, as they prefer shallower and calmer waters. Pool 2 is found in the center of Banizoumbou and is photographed in Figure 3. This pool is a productive mosquito breeding site, which, combined with its proximity to households, makes it a significant public health concern. Pool 3 is another typical pool where mosquito larvae are found.

[15] The entomology component of HYDREMATS simulates individual mosquito and human agents. Human agents are immobile and are assigned to village residences, as malaria transmission in this region occurs primarily at night when humans are indoors [*Service*, 1993]. Mosquito agents have a probabilistic response to their environment based on a prescribed set of rules governing dispersal and discrete events, including development of larval stages, feeding, egg laying, and death. The model tracks the location, feeding status, and reproductive status of each female mosquito through time. General trends and relative abundances of simulated mosquito abundances compare well to field captures of mosquitoes in Banizoumbou [*Bomblies et al.*, 2008].

[16] In addition to the water pool inputs supplied by the hydrology component of the model, the entomology component requires air temperature, humidity, wind speed, and wind direction. Air temperature and relative humidity influence mosquito behavior and survival, while wind speed and direction influence mosquito flight, both by physical displacement by wind and by attracting mosquitoes to

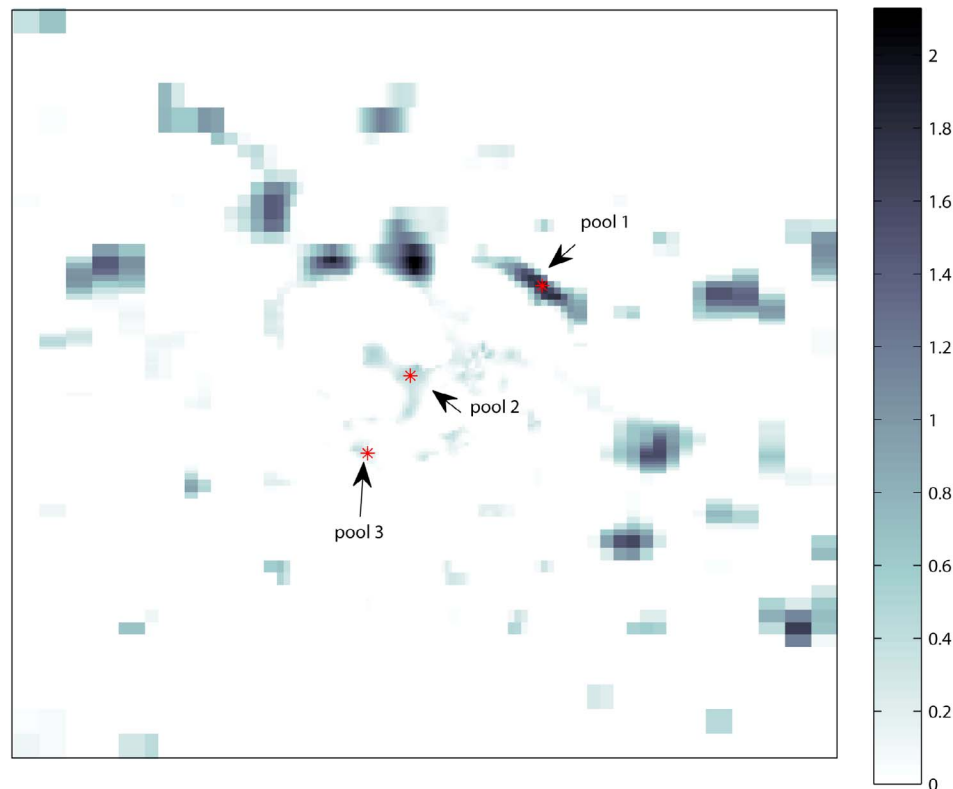


**Figure 2.** Pool depth output in meters for the  $2.5 \times 2.5$  km Banizoumbou domain for a sample time step.

upwind blood sources. The location of village residences is required in order to assign the location of human agents [Bomblies *et al.*, 2008].

[17] Mosquito eggs hatch and advance through four stages of larval development at rates dependent on water temperature, nutrient competition, and predation given by Depinay *et al.* [2004]. Surviving larvae pupate and emerge as adult mosquitoes. The duration of the aquatic stage of *A. gambiae* mosquitoes ranges from 8 to 24 days [Depinay *et al.*, 2004]. All aquatic stage mosquitoes in a pool that dries up are killed, emphasizing the importance of pool persistence for mosquito breeding [Bomblies *et al.*, 2008]. Adult female mosquitoes follow a cycle of seeking human blood meals, feeding, resting, and ovipositing for the duration of their lifespan. Mosquito flight velocity is assigned as a weighted random walk corrected for attraction to upwind  $\text{CO}_2$  and wind influence. The effective flight velocity, which incorporates resting time and direction changes within the model time step, is assumed to follow a normal distribution with mean 15 m/h and variance 25 m/h. Mortality of adult mosquitoes is a function of daily average temperature, with no survival above a daily average temperature of  $41^\circ\text{C}$ .

[18] The model also includes a malaria component that represents the stages of the malaria life cycle. However, this aspect of the model has not yet been validated with field data. The malaria parasite is transmitted to a mosquito when the mosquito bites an infected human. It develops within the mosquito at a temperature dependant rate described by Detinova [1962] and is transmitted back to a human when the infected mosquito takes a blood meal from an uninfected human. The human infections clear with time. The model

outputs for each time step includes the number of live adult mosquitoes, their location and infective status, and the prevalence of malaria infections in humans [Bomblies *et al.*, 2008].

[19] While HYDREMATS can be used to assess the potential for malaria transmission on the basis of the climatic determinants of disease transmission, actual levels of malaria transmission depend on many more factors, including the presence of the parasite within a population, local vector control activities, access to medical service, differences in host susceptibility, and movement of people in and out of the modeled population.

## 4. The Effect of the Temporal Resolution of Precipitation on Simulations of Mosquito Populations Using HYDREMATS

### 4.1. Simulation Description

[20] The meteorological station in Banizoumbou is owned and operated by Institut de Recherche pour le Développement (IRD). Rainfall data are collected by a tipping bucket rain gauge at 5 min intervals. To examine the model's sensitivity to the temporal resolution of rainfall, the 5 min rainfall data during the rainy season of the year 2006 were aggregated to construct rainfall data sets with 15 min, 30 min, 1 h, 3 h, 6 h, 12 h, and 24 h resolutions. HYDREMATS simulations were conducted for each rainfall data set, operating at a 15 min time step, from 1 June 2006 through 31 October 2006. The total rainfall measured during this time was 505.55 mm. The 15 min resolution rainfall measurements were assumed to be



**Figure 3.** Pool 2, located in the center of Banizoumbou village, is a typical mosquito breeding site.

the truth, and the simulation using 15 min rainfall resolution served as the control simulation. Rainfall inputs for the 30 min and lower-resolution data sets were prepared by distributing the aggregate data rainfall equally into 15 min periods. For example, the 1 h resolution rainfall input was constructed by distributing the total rainfall for the first hour over four 15 min intervals, followed by the total rainfall for the second hour divided over four 15 min intervals. Simulations were not conducted using the original 5 min rainfall resolution because of the computational time requirements of using a 5 min time step. All other meteorological inputs, temperature, humidity, wind speed and direction, and radiation, had a 1 h resolution and did not vary between simulations. The model domain was a  $2.5 \text{ km} \times 2.5 \text{ km}$  area centered over Banizoumbou village.

## 4.2. Results

### 4.2.1. Effect on Water Pools

[21] Model outputs for total mass of pooled water, total pool surface area, water levels of three specific pools, evaporation, infiltration, and mosquito populations were analyzed by Yamana [2010]. The total mass of pooled water at each time step in the 30 min, 1 h, and 3 h rainfall resolution scenarios were highly correlated with the control scenario (correlation coefficient  $>0.97$ ). However, quantity of water stored in pools at each time step decreases as rainfall resolution decreases further. Despite the high correlation of mass of pooled water, the cumulative sum of

pooled water over the entire rainy season is nearly 20% less than the control in the 1 h simulation and nearly 50% less than the control in the 3 h simulation. Averaging rainfall over 24 h results in a cumulative total of pooled water of only 0.3% of the amount in the control simulation, with a correlation coefficient of less than 0.005.

[22] The surface area of water pools is an important characteristic, as larvae are limited to the water surface. The total surface area of water pools over the model domain can be calculated by counting the number of grid points with water depth above a threshold value. The scatterplots in Figure 4 compare the proportion of the model domain covered in pools at the beginning of each day in the control simulation on the  $x$  axis to that in the 30 min, 1 h, 3 h, and 6 h simulations on the  $y$  axis. Figure 4 shows that daily outputs of surface area in the 30 min and 1 h scenarios correspond well with the control, while the 3 h and 6 h resolution scenarios significantly underestimate the surface area of water pools. This is consistent with the decreasing volume of pooled water observed in these coarse-resolution scenarios. As with the mass of pooled water, we see that the surface area of water pools decreases as the temporal resolution of rainfall coarsens. The correlation coefficient between the simulations and control decreases at a faster rate for surface area than it does for water mass, decreasing to 0.91 for the 1 h simulation and 0.80 for the 3 h simulation. The results are similar when the surface area considered is restricted to shallow waters preferred by mosquitoes, which is set in the model to be water less than 0.7 m deep. The correlation coefficients between the

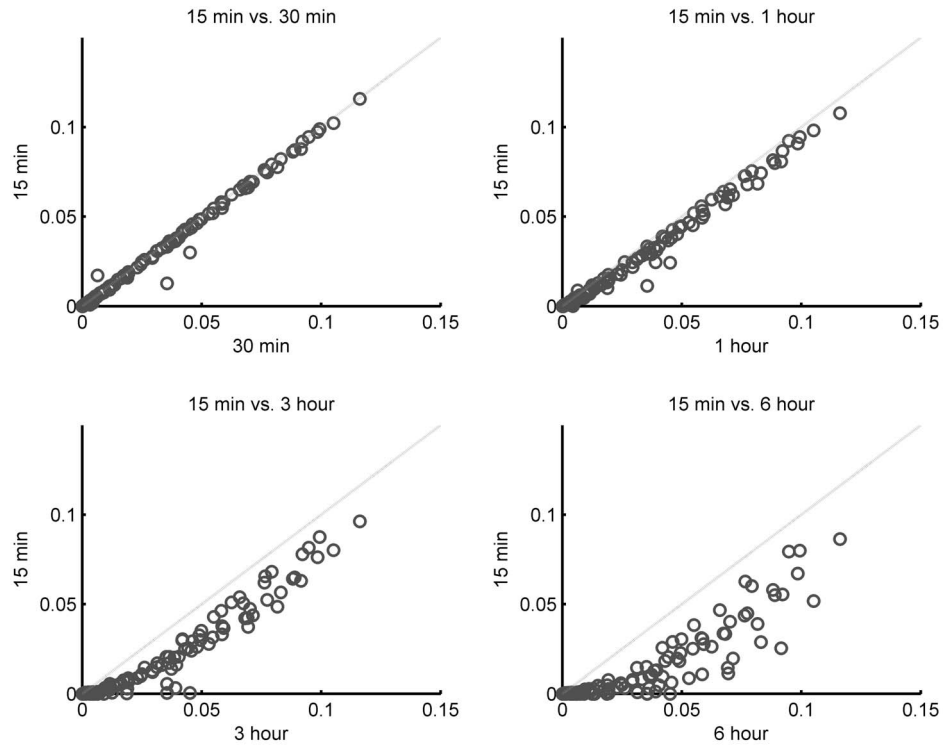


**Figure 4.** Daily proportion of pooled area. Outputs from the control simulation are shown on the y axes, while outputs from the 30 min, 1 h, 3 h, and 6 h simulations are shown on the x axes.

simulations and control for the surface area of shallow water were 1.00, 0.99, 0.90, and 0.82 for the 30 min, 1 h, 3 h, and 6 h simulations, respectively.

[23] The decrease in both the surface area and volume of pooled water observed when the model is run with coarse rainfall resolution can be explained by the differences in rainfall intensity between the scenarios. In the control simulation, rainfall events occur as short-duration, high-intensity events, with rain falling at a faster rate than can be absorbed by the soil. This leads to runoff and pool formation. When these rainfall events are averaged over 1 or more hours, the events begin to resemble long-duration, low-intensity rainfall, which is more easily infiltrated into the soil.

#### 4.2.2. Effect on Mosquito Population

[24] Figure 5 shows the number of female adult mosquitoes alive at each time step for the different simulations. We see that the number of mosquitoes in the 30 min, 1 h, and 3 h simulations is very highly correlated to the number in the control simulation, with a correlation coefficient of  $\geq 0.95$ . While the peaks and ebbs are closely matched between the various simulations, the coarser resolutions significantly underestimate the magnitude of mosquito populations. The number of adult mosquitoes at each time step in the 30 min and 1 h simulations corresponds reasonably well with the control, underestimating the cumulative sum of mosquitoes by 12% and 15%, respectively. The majority of this underestimation occurs in the first three peaks in the mosquito populations, occurring between late mid-July and late August. When the rainfall resolution is degraded to 3 h resolution, the model shows the cumulative sum of live mosquitoes as less than 50% of that in the control. This dramatic drop in mosquito populations reflects the decrease in surface area

of pooled water, as pooled water drops from 90% the amount seen in the control at 1 h resolution to 66% of the control at 3 h resolution. When the rainfall is averaged over 12 or 24 h, the resulting simulations show only very minimal mosquito breeding, with the cumulative sum of mosquitoes being 13% and 7%, respectively, of that of the control.

#### 4.3. Discussion

[25] Hydrological modeling can add valuable information to malaria transmission models. However, in order to function properly, these models require a fine temporal resolution of rainfall inputs. These simulations show that while the availability and convenience of using a rainfall data set with low temporal resolution has certain advantages, HYDREMATS' skill in accurately modeling the hydrologic and entomologic systems decreases as the resolution of rainfall decreases. This is because low temporal resolution data sets average rainfall events into longer, lower-intensity events that lead to more infiltration and reduce the amount of pooling. The decreased amount of water in pools means that there is less breeding habitat available for mosquitoes, and thus, the number of mosquitoes decreases.

[26] Given the results of these simulations, we conclude that a minimum rainfall resolution of 1 h should be used with HYDREMATS. Although there is some loss in accuracy, the high levels of correlation of all examined variables between the 1 h simulation and the control indicate that HYDREMATS can give a reasonable representation of the environment using rainfall inputs of this resolution. Meanwhile, 1 h resolution data are likely to be more available than rainfall data with finer resolution. While 3 h and coarser resolution rainfall data sets are even more widely

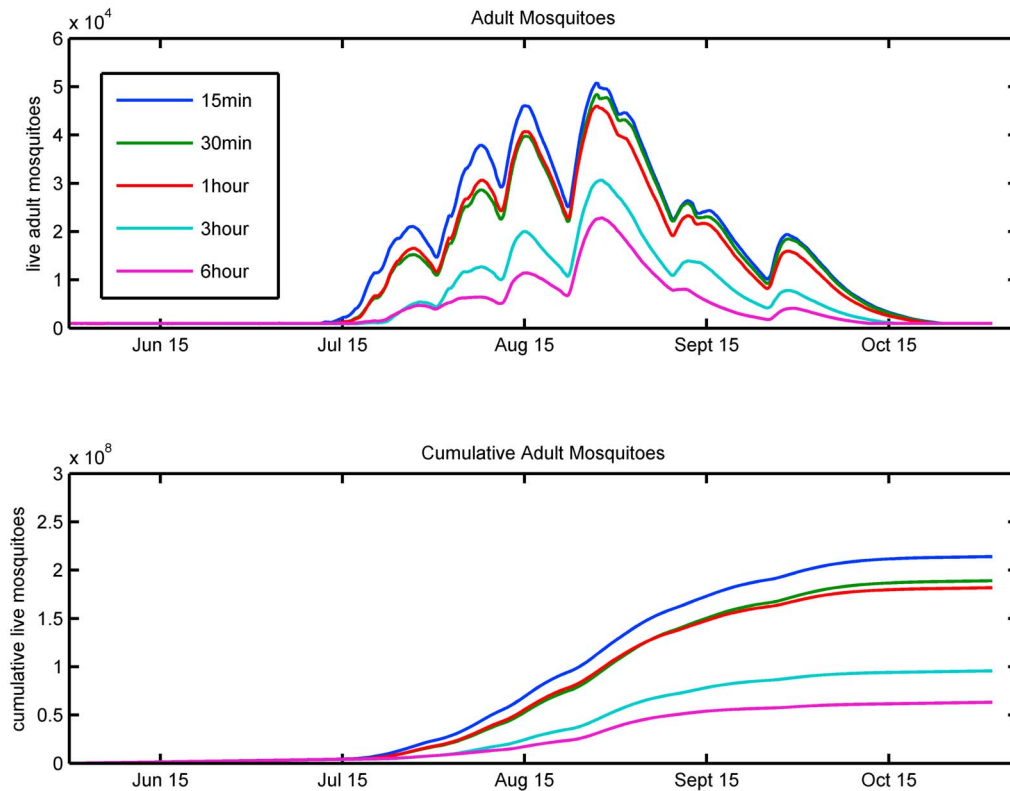


Figure 5. Adult female mosquitoes from each of the simulations.

available, using these data sets would result in significant losses in the accuracy of the model.

## 5. Application of Satellite Estimates of Rainfall Distribution to Simulate the Potential for Malaria Transmission in Africa

### 5.1. Calibrating CMORPH Rainfall Estimates

[27] Here, we use CMORPH data instead of ground observations as the rainfall forcing in HYDREMATS for Banizoumbou, Niger, in 2007. We first developed a simple method of correcting for the wet bias in CMORPH on the basis of rules made by comparing CMORPH to ground data at three locations in West Africa in 2006: Zindarou in Niger, Agoufou in Mali, and Djougou in Benin. Data from Banizoumbou were not used in the calibration process. Rainfall in Zindarou was measured using a Texas Electronics TE525 rain gauge, installed by *Bombliès et al.* [2008] and maintained by Centre de Recherche Médicale et Sanitaire, our collaborators in Niger. Rain gauge data for the other three locations were provided by IRD of Niger, Mali, and Benin and were obtained through the African Monsoon and Multidisciplinary Analyses (AMMA) database. CMORPH values used for each village corresponded to the roughly 8 km by 8 km CMORPH grid cell containing the coordinates of each rain gauge. The 30 min CMORPH data and 5–20 min rain gauge data for these four locations were averaged into hourly values of rainfall, which is the time step determined by the previous investigation to be sufficient for accurate use of HYDREMATS.

[28] An initial comparison of rainfall totals between the two types of data sets showed that CMORPH overestimated total annual rainfall by 45%–68%. The frequency bias (FB), false alarm ratio (FAR), and probability of detection (POD) were calculated on hourly and daily time scales. The FB refers to the number of hours or days where CMORPH estimates nonzero rainfall divided by the number of nonzero rainfall observations on the ground. FAR refers to the fraction of nonzero rainfall estimates in CMORPH that did not correspond to nonzero rainfall measurements on the ground. The POD is the fraction of nonzero rainfall measurements observed on the ground that were correctly detected by CMORPH. The POD, FB, and FAR for hourly and daily data at each location were analyzed by *Yamana* [2010]. The overall FB was 1.81 for hourly data and 1.31 for daily data. This means that CMORPH estimates far more nonzero rainfall hours than are actually observed on the ground. The significant lowering of FB when rainfall is averaged over 24 h implies that many of the false positives could be the result of overestimating the length of actual rainfall events. The POD over all four sites is 0.61 on the hourly scale and 0.81 on the daily scale. The FAR is 0.67 hourly and 0.38 daily.

[29] Examining the data, we observed that many of the false positives occurred when the CMORPH hourly rainfall estimates were less than 1 mm. Such small amounts of rainfall are likely to evaporate before reaching the surface. It was found that the FB and FAR could be significantly reduced by setting all CMORPH data points less than or equal to 0.4–0 mm, with a tradeoff being a small decrease in the POD. On the hourly scale, this adjustment led to a 33% decrease in FB, a 15% decrease in the FAR, and a 15%

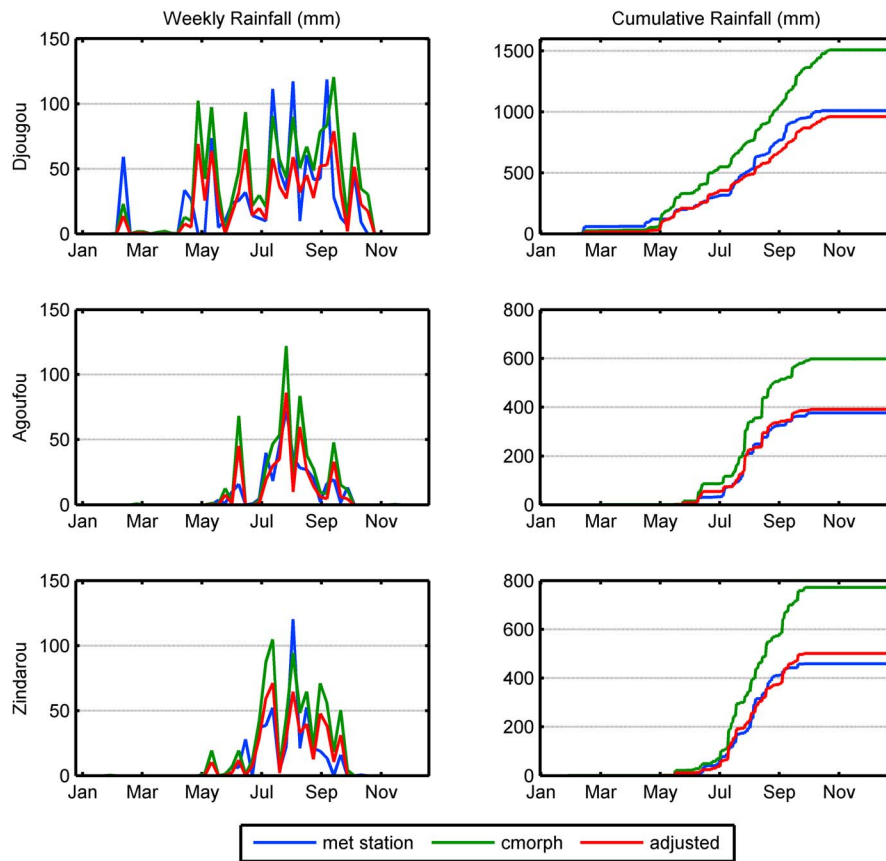


**Figure 6.** Weekly and cumulative rainfall in 2006. Ground observations are shown in blue, raw CMORPH data are shown in green, and adjusted CMORPH data are shown in red.

decrease in the POD. On the daily time scale, the FB and the FAR decreased by 11%, while the POD decreased by 5%.

[30] After removing the low-intensity rainfall estimates, CMORPH data were further adjusted by multiplying each value by the ratio of total rainfall measured by rain gauges to total rainfall estimated by CMORPH in Zindarou, Agoufou, and Djougou, which was 0.73. Banizoumbou was not included in the calculation of the correction factor so that we could test the applicability of the adjustment method to other stations. This crude adjustment scaled down CMORPH estimates such that the annual totals were closer in magnitude to observed data. Figure 6 shows weekly and cumulative rainfall for the three locations for rain gauge data, raw CMORPH data, and adjusted CMORPH data. We see that the adjusted CMORPH data set agrees well with yearly rainfall totals and, in many cases, with weekly rainfall totals.

[31] The adjustment method was applied to CMORPH data for Banizoumbou in 2007. The resulting rainfall series, shown in Figure 7, was the rainfall forcing for the CMORPH simulation in HYDREMATS. The correlation between the adjusted CMORPH rainfall and meteorological station rainfall during the rainy season (1 June 1 to 31 October) was 0.26, 0.74, and 0.77 for the hourly, daily, and weekly time scales, respectively.

## 5.2. Simulation Description

[32] This investigation was based on two HYDREMATS simulations conducted over the domain of Banizoumbou,

Niger, for the year 2007. The first simulation, the control, used rain gauge data as the rainfall input. The second simulation used adjusted CMORPH data as the rainfall forcing. The simulations ran using a 1 h time step.

## 5.3. Results

[33] The hourly depths of the three pools described in Figure 2 are presented in Figure 8, with the blue line depicting pool depth output from the simulation using ground data and the red line pool depth using adjusted CMORPH rainfall forcings. Pool 1, the deepest and largest of the pools, was consistently deeper in the ground data simulation than in the CMORPH simulation, despite the fact that the CMORPH simulation had slightly more total rainfall. The depths of pools 2 and 3 are closer in magnitude between the two simulations, but their correlations are lower. The correlation coefficients between the two simulations are 0.99, 0.78 and 0.83 for Pools 1, 2, and 3 respectively.

[34] The initial disparity of depths between the two simulations observed in pool 1, observed mid-June, is interesting because it accentuates the importance of rainfall distribution in the pool formation process. The rainfall event leading to the formation of pool 1 occurred over a 9 h period between 15 and 16 June 2007. This event was recorded by both the rain gauge and CMORPH, with the rain gauge showing a total of 40.5 mm, while the adjusted CMORPH data set showed a total of 39.6 mm rainfall. Despite this very close agreement in magnitude of the event, the gauge data recorded the rainfall



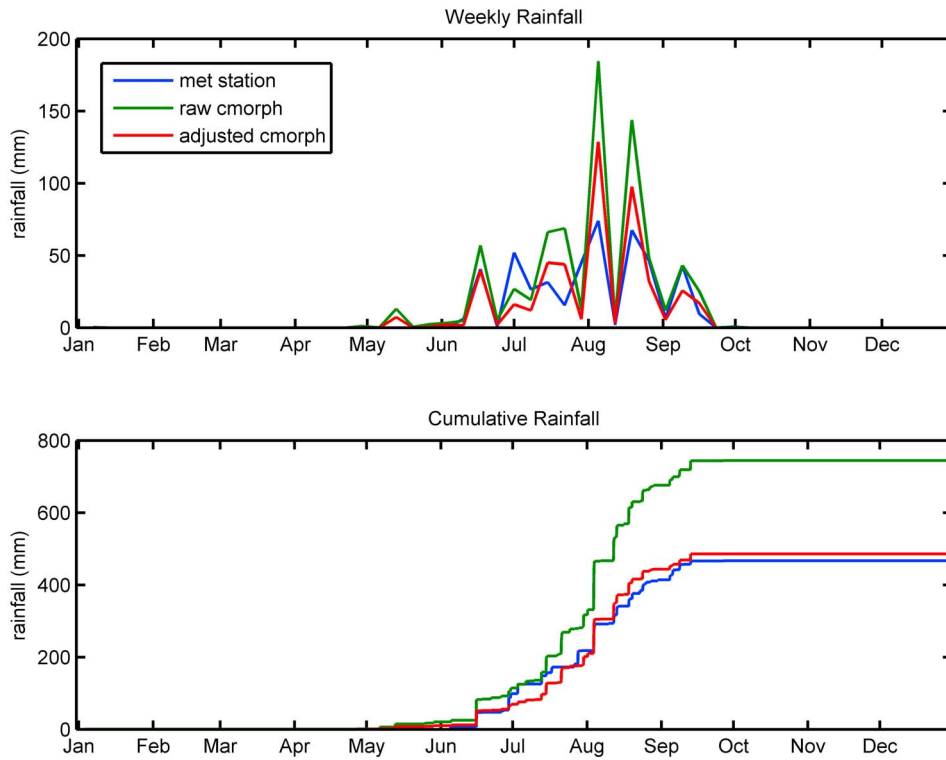


**Figure 7.** Banizoumbou weekly rainfall in 2007. Ground observations are shown in blue, raw CMORPH data are shown in green, and adjusted CMORPH data are shown in red.

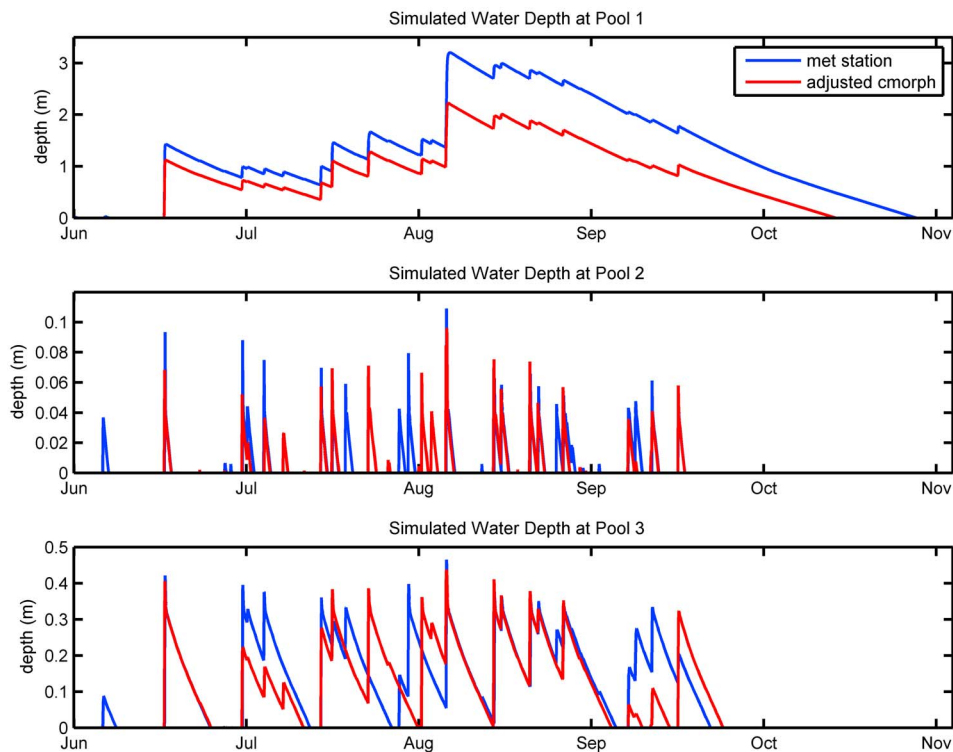


**Figure 8.** Water levels at three pools. The blue lines correspond to depths simulated in the control simulation, while the red lines show depths simulated in the adjusted CMORPH simulation.

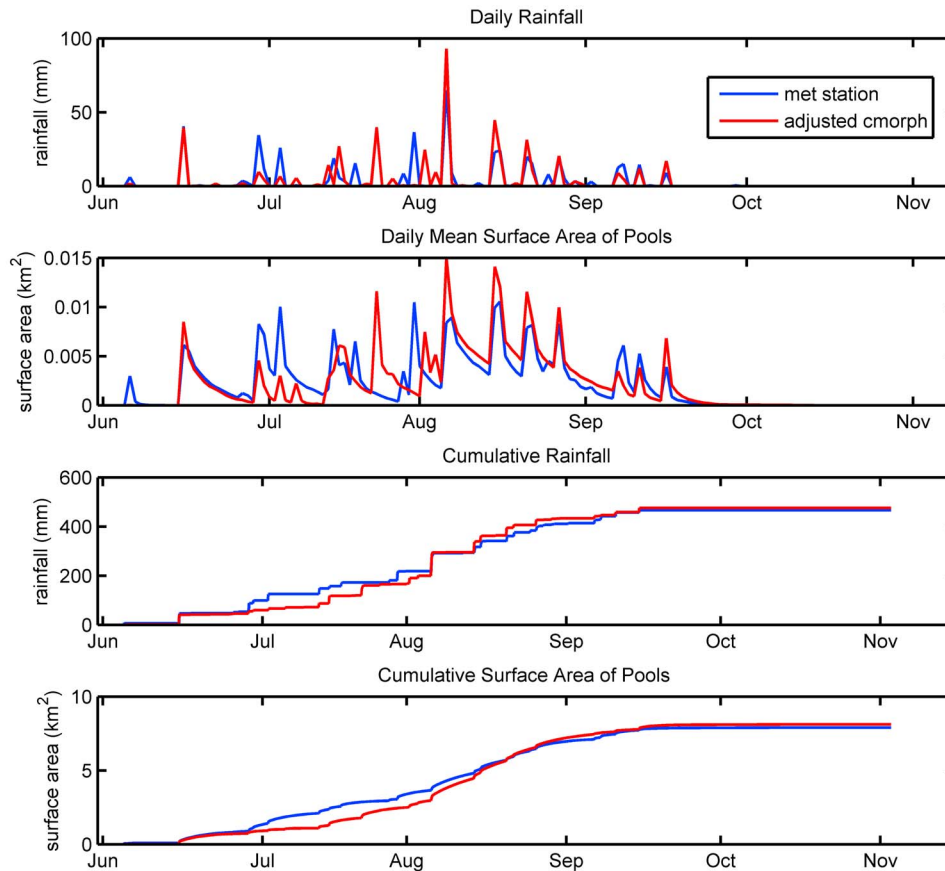


**Figure 9.** Daily rainfall inputs and surface area outputs from the control (blue) and CMORPH (red) simulations.

over 3 h with a maximum intensity of 34.6 mm/h, while the adjusted CMORPH data showed the event as occurring over 7 h with a maximum intensity of 16.1 mm/h. The higher intensity rainfall in the rain gauge simulation caused higher rates of surface runoff, leading to greater volumes of pooled water; thus, pool 1 was deeper in the rain gauge simulation than it was in the CMORPH simulation. The same reason explains the increased difference in depths of pool 1 observed in early August. Pools 2 and 3 are much smaller and shallower and are therefore less sensitive to the overall runoff patterns of the model domain. They quickly reach their maximum depth, after which excess water travels as runoff to a greater depression in the topography.

[35] While differences in rainfall distribution accounted for the discrepancies seen in pool 1 in mid-June and early August, this is not representative of all rainfall events. Figure 9 shows the daily mean surface area of pools, cumulative surface area of pools, and cumulative rainfall. There is significant correlation between the daily mean surface area of water pools of the two simulations, with a correlation coefficient of 0.76. This correlation is comparable to that of rainfall at the daily time scale. Comparing cumulative surface area of pools to cumulative rainfall shows that the major discrepancies observed in the daily mean surface area of pools between the two simulations are primarily due to differences in the magnitude of rainfall events between the adjusted CMORPH and ground data rather than differences in their temporal distribution; the

surface area of pools is closely correlated to rainfall, with a correlation coefficient of 0.76 in the meteorological station simulation and 0.84 in the CMORPH simulation.

[36] The number of live female mosquitoes simulated at each time step for the two simulations is shown in Figure 10. The correlation coefficient for the two outputs is 0.98, and the root-mean-square error is  $5.9 \times 10^3$ . The CMORPH simulation shows lower numbers of mosquitoes than the rain gauge simulation in late June and July and early September and greater numbers in August. This is consistent with the relative amounts of pooled water available during these times under the two model simulations.

#### 5.4. Discussion

[37] The results of this study demonstrate that satellite-derived estimates of rainfall can be used in a mechanistic model to simulate mosquito populations and malaria transmission. The use of satellite data with such models has been described as the logical next step to existing studies using satellite data for malaria control [Rogers *et al.*, 2002; Kalluri *et al.*, 2007]. While studies that use statistical information to infer relationships between satellite-based environmental observations and malaria transmission have great value in mapping malaria risk areas on the country scale, they generally do not address village-scale variability. Since they most often do not explain causal pathways between remotely sensed data and malaria transmission, they have

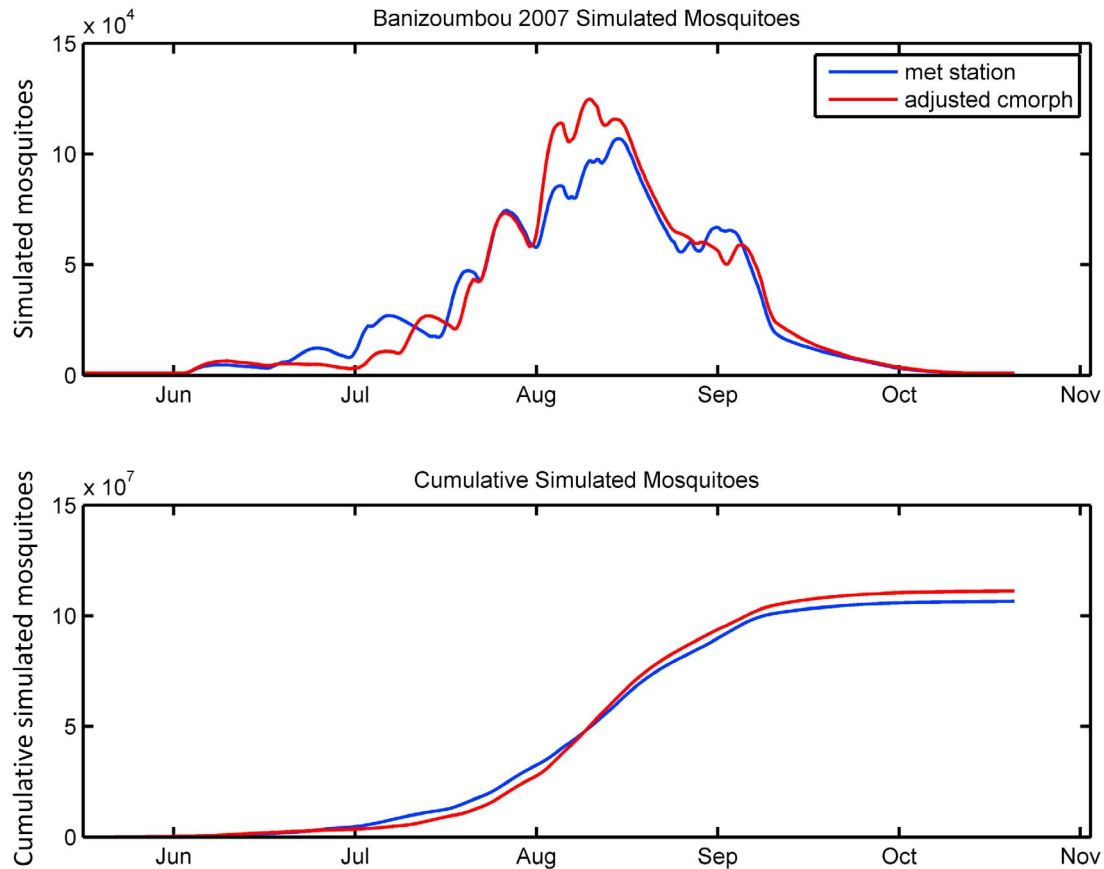


**Figure 10.** Hourly outputs of adult female mosquitoes from the control (blue) and CMORPH (red) simulations.

limited ability to predict the malaria response to a given environmental change.

[38] Satellite technology is constantly improving, providing plentiful information which can be used in a model such as ours. In the future, we envision a system by which most of the inputs to HYDREMATS could be obtained by satellite and archived data sets. These inputs include temperature, humidity, wind speed and direction, topography, soil characteristics, and location of residences. If these data could all be applied to the model, the range of applicability of HYDREMATS could be extended to every village in western Africa as well as any other area where malaria transmission is limited by the availability of water. HYDREMATS could be a valuable tool for researchers and those working in malaria control programs. This would be especially useful for addressing changes in the environment such as climate change and land use change.

## 6. Conclusion

[39] We have demonstrated that hydrology-based mechanistic models of malaria transmission require rainfall data with at least 1 h resolution. This requirement is far greater than the rainfall inputs used by previous modeling studies of malaria transmission. This resolution allows accurate modeling of pool formation processes that form the link between rainfall and mosquito abundance. While ground observations with 1 h resolutions may be difficult to obtain in many malaria-prone

areas, we have shown that satellite data can be used as the rainfall forcing. After applying a simple adjustment, we demonstrate that CMORPH satellite data are of sufficient resolution and accuracy to be used with HYDREMATS. This presents a new use for satellite estimates of rainfall, as a forcing of a mechanistic model to simulate mosquito populations.

[40] **Acknowledgments.** AMMA, which is based on a French initiative, was built by an international scientific group and is currently funded by a large number of agencies, especially from France, the United Kingdom, the United States, and Africa. It has been the beneficiary of a major financial contribution from the European Community's Sixth Framework Research Programme. The authors thank the anonymous reviewers for their helpful comments. This work was funded by U.S. National Science Foundation grants EAR-0946280 and EAR-0824398.

## References

- Aregawi, M., R. Cibulskis, and M. Otten (2008), World malaria report 2008, World Health Organ., Geneva, Switzerland.
- Beck, L. R., M. H. Rodriguez, S. W. Dister, A. D. Rodriguez, E. Rejmankova, A. Ulloa, R. A. Meza, D. R. Roberts, J. F. Paris, and M. A. Spanner (1994), Remote sensing as a landscape epidemiologic tool to identify villages at high risk for malaria transmission, *Am. J. Trop. Med. Hyg.*, 51, 271–280.
- Bogh, C., S. W. Lindsay, S. E. Clarke, A. Dean, M. Jawara, M. Pinder, and C. J. Thomas (2007), High spatial resolution mapping of malaria transmission risk in the Gambia, West Africa, using LANDSAT TM satellite imagery, *Am. J. Trop. Med. Hyg.*, 76, 875–881.
- Bombliès, A., and E. A. B. Eltahir (2010), Assessment of the impact of climate shifts on malaria transmission in the Sahel, *EcoHealth*, 6, 426–437, doi:10.1007/s10393-010-0274-5.

- Bomblics, A., J. B. Duchemin, and E. A. B. Eltahir (2008), Hydrology of malaria: Model development and application to a Sahelian village, *Water Resour. Res.*, *44*, W12445, doi:10.1029/2008WR006917.
- Ceccato, P., S. Connor, I. Jeanne, and M. Thomson (2005), Application of geographical information systems and remote sensing technologies for assessing and monitoring malaria risk, *Parassitologia*, *47*, 81–96.
- Ceccato, P., M. Bell, M. Blumenthal, S. Connor, T. Dinku, E. Grover-Kopec, C. Ropelewski, and M. Thomson (2006), Use of remote sensing for monitoring climate variability for integrated early warning systems: Applications for human diseases and desert locust management, paper presented at International Conference on Geoscience and Remote Sensing Symposium, Inst. of Electr. and Electron. Eng., Denver, Colo.
- Craig, M. H., R. W. Snow, and D. le Sueur (1999), A climate-based distribution model of malaria transmission in sub-Saharan Africa, *Parasitol. Today*, *15*, 105–111, doi:10.1016/S0169-4758(99)01396-4.
- Depinay, J. M., et al. (2004), A simulation model of African *Anopheles* ecology and population dynamics for the analysis of malaria transmission, *Malar. J.*, *3*, 29, doi:10.1186/1475-2875-3-29.
- Detinova, T. S. (1962), Age-grouping methods in Diptera of medical importance, with special reference to some vectors of malaria, *WHO Monogr. Ser.* *47*, 216 pp., World Health Organ, Geneva, Switzerland.
- Diuk-Wasser, M., M. Bagayoko, N. Sogoba, G. Dolo, M. Touré, S. Traoré, and C. Taylor (2004), Mapping rice field anopheline breeding habitats in Mali, West Africa, using Landsat ETM sensor data, *Int. J. Remote Sens.*, *25*, 359–376, doi:10.1080/01431160310001598944.
- Eisele, T. P., J. Keating, C. Swalm, C. M. Mbogo, A. K. Githeko, J. L. Regens, J. I. Githure, L. Andrews, and J. C. Beier (2003), Linking field-based ecological data with remotely sensed data using a geographic information system in two malaria endemic urban areas of Kenya, *Malar. J.*, *2*, 44, doi:10.1186/1475-2875-2-44.
- Finnerty, B. D., M. B. Smith, D. J. Seo, V. Koren, and G. E. Moglen (1997), Space-time scale sensitivity of the Sacramento model to radar-gage precipitation inputs, *J. Hydrol.*, *203*, 21–38, doi:10.1016/S0022-1694(97)00083-8.
- Gianotti, R., A. Bomblics, and E. Eltahir (2008a), Using hydrologic modeling to screen potential environmental management methods for malaria vector control in Niger, *Eos Trans. AGU*, *89*(53), Fall Meet. Suppl., Abstract B53B-0494.
- Gianotti, R. L., A. Bomblics, M. Dafalla, I. Issa-Arzika, J. B. Duchemin, and E. A. Eltahir (2008b), Efficacy of local neem extracts for sustainable malaria vector control in an African village, *Malar. J.*, *7*, 138, doi:10.1186/1475-2875-7-138.
- Grover-Kopec, E., M. Kawano, R. W. Klaver, B. Blumenthal, P. Ceccato, and S. J. Connor (2005), An online operational rainfall-monitoring resource for epidemic malaria early warning systems in Africa, *Malar. J.*, *4*, 6, doi:10.1186/1475-2875-4-6.
- Hay, S. I., R. W. Snow, and D. J. Rogers (1998a), Predicting malaria seasons in Kenya using multitemporal meteorological satellite sensor data, *Trans. R. Soc. Trop. Med. Hyg.*, *92*, 12–20, doi:10.1016/S0035-9203(98)90936-1.
- Hay, S., R. Snow, and D. Rogers (1998b), From predicting mosquito habitat to malaria seasons using remotely sensed data: Practice, problems and perspectives, *Parasitol. Today*, *14*, 306–313, doi:10.1016/S0169-4758(98)01285-X.
- Hay, S. I., E. C. Were, M. Renshaw, A. M. Noor, S. A. Ochola, I. Olusanmi, N. Alipui, and R. W. Snow (2003), Forecasting, warning, and detection of malaria epidemics: A case study, *Lancet*, *361*, 1705–1706, doi:10.1016/S0140-6736(03)13366-1.
- Hoshen, M., and A. Morse (2004), A weather-driven model of malaria transmission, *Malar. J.*, *3*, 32, doi:10.1186/1475-2875-3-32.
- Joyce, R. J., J. E. Janowiak, P. A. Arkin, and P. Xie (2004), CMORPH: A method that produces global precipitation estimates from passive microwave and infrared data at high spatial and temporal resolution, *J. Hydrometeorol.*, *5*, 487–503, doi:10.1175/1525-7541(2004)005<0487:CAMTPG>2.0.CO;2.
- Kalluri, S., P. Gilruth, D. Rogers, and M. Szczur (2007), Surveillance of arthropod vector-borne infectious diseases using remote sensing techniques: A review, *PLoS Pathog.*, *3*, 1361–1371, doi:10.1371/journal.ppat.0030116.
- Kilian, A. H. D., P. Langi, A. Talisuna, and G. Kabagambe (1999), Rainfall pattern. El Niño and malaria in Uganda, *Trans. R. Soc. Trop. Med. Hyg.*, *93*, 22–23, doi:10.1016/S0035-9203(99)90165-7.
- Krajewski, W. F., V. Lakshmi, K. P. Georgakakos, and S. C. Jain (1991), A Monte Carlo study of rainfall sampling effect on a distributed catchment mode, *Water Resour. Res.*, *27*, 119–128.
- Lal, A. M. W. (1998), Performance comparison of overland flow algorithms, *J. Hydraul. Eng.*, *124*, 342–349, doi:10.1061/(ASCE)0733-9429(1998)124:4(342).
- Laws, K. B., J. E. Janowiak, and G. Huffman (2004), Verification of rainfall estimates over Africa using RFE, NASA MAPRT-RT and CMORPH, paper presented at 84th Annual Meeting, Am. Meteorol. Soc., Seattle, Wash., 11–15 Jan.
- Masuoka, P. M., D. M. Claborn, R. G. Andre, J. Nigro, S. W. Gordon, T. A. Klein, and H. C. Kim (2003), Use of IKONOS and Landsat for malaria control in the Republic of Korea, *Remote Sens. Environ.*, *88*, 187–194, doi:10.1016/j.rse.2003.04.009.
- Nihei, N., Y. Hashida, M. Kobayashi, and A. Ishii (2002), Analysis of malaria endemic areas on the Indochina Peninsula using remote sensing, *Jpn. J. Infect. Dis.*, *55*, 160–166.
- Omumbo, J., S. Hay, S. Goetz, R. Snow, and D. Rogers (2002), Updating historical maps of malaria transmission intensity in East Africa using remote sensing, *Photogramm. Eng. Remote Sens.*, *68*, 161–166.
- Patz, J. A., K. Strzepek, S. Lele, M. Hedden, S. Greene, B. Noden, S. I. Hay, L. Kalkstein, and J. C. Beier (1998), Predicting key malaria transmission factors, biting and entomological inoculation rates, using modelled soil moisture in Kenya, *Trop. Med. Int. Health*, *3*, 818–827, doi:10.1046/j.1365-3156.1998.00309.x.
- Pessoa, M. L., R. L. Bras, and E. R. Williams (1993), Use of weather radar for flood forecasting in the Sieve River basin: A sensitivity analysis, *J. Appl. Meteorol.*, *32*, 462–475, doi:10.1175/1520-0450(1993)032<0462:UOWRFF>2.0.CO;2.
- Pollard, D., and S. L. Thompson (1995), Use of a land-surface-transfer scheme (LSX) in a global climate model: The response to doubling stomatal resistance, *Global Planet. Change*, *10*, 129–161, doi:10.1016/0921-8181(94)00023-7.
- Pope, K. O., E. Rejmankova, H. M. Savage, J. I. Arredondo-Jimenez, M. H. Rodriguez, and D. R. Roberts (1994), Remote sensing of tropical wetlands for malaria control in Chiapas, Mexico, *Ecol. Appl.*, *4*, 81–90, doi:10.2307/1942117.
- Rahman, A., F. Kogan, and L. Roytman (2006), Analysis of malaria cases in Bangladesh with remote sensing data, *Am. J. Trop. Med. Hyg.*, *74*, 17–19.
- Rogers, D. J., S. E. Randolph, R. W. Snow, and S. I. Hay (2002), Satellite imagery in the study and forecast of malaria, *Nature*, *415*, 710–715, doi:10.1038/415710a.
- Service, M. (1993), *Mosquito Ecology: Field Sampling Methods*, 2nd ed., Elsevier Appl. Sci., London.
- Thomson, M. C., S. J. Connor, P. J. Milligan, and S. P. Flasse (1996), The ecology of malaria—As seen from Earth-observation satellites, *Ann. Trop. Med. Parasitol.*, *90*, 243–264.
- Thomson, M., S. Connor, U. D'Alessandro, B. Rowlingson, P. Diggle, M. Cresswell, and B. Greenwood (1999), Predicting malaria infection in Gambian children from satellite data and bed net use surveys: The importance of spatial correlation in the interpretation of results, *Am. J. Trop. Med. Hyg.*, *61*, 2–8.
- Thomson, M. C., S. J. Mason, T. Phindela, and S. J. Connor (2005), Use of rainfall and sea surface temperature monitoring for malaria early warning in Botswana, *Am. J. Trop. Med. Hyg.*, *73*, 214–221.
- Tian, Y., and C. D. Peters-Lidard (2007), Systematic anomalies over inland water bodies in satellite-based precipitation estimates, *Geophys. Res. Lett.*, *34*, L14403, doi:10.1029/2007GL030787.
- Winchell, M., H. V. Gupta, and S. Sorooshian (1998), On the simulation of infiltration-and saturation-excess runoff using radar-based rainfall estimates: Effects of algorithm uncertainty and pixel aggregation, *Water Resour. Res.*, *34*, 2655–2670, doi:10.1029/98WR02009.
- Yamana, T. K. (2010), Simulations and predictions of mosquito populations in Africa using rainfall inputs from satellites and forecasts, M.S. thesis, Dep. of Civ. and Environ. Eng., Mass. Inst. of Technol., Cambridge, Mass.

E. A. B. Eltahir and T. K. Yamana, Ralph M. Parsons Laboratory, Massachusetts Institute of Technology, 15 Vassar St., Cambridge, MA 02139, USA. (tkcy@mit.edu)